Guobiao Hu
Department of Mechanical Engineering,
University of Auckland,
20 Symonds Street,
Auckland 1010, New Zealand
e-mail: ghu211@aucklanduni.ac.nz

Lihua Tang[1]
Department of Mechanical Engineering,
University of Auckland,
20 Symonds Street,
Auckland 1010, New Zealand
e-mail: l.tang@auckland.ac.nz

Jiawen Xu
Jiangsu Key Lab of Remote Measurement and Control,
School of Instrument Science and Engineering,
Southeast University,
Nanjing, Jiangsu 210096, China
e-mail: jiawen.xu@seu.edu.cn

Chunbo Lan
College of Aerospace Engineering,
Nanjing University of Aeronautics and Astronautics,
Nanjing, Jiangsu 210016, China
e-mail: chunbolan@nuaa.edu.cn

Raj Das
School of Engineering,
RMIT University,
GPO Box 2476,
Melbourne, VIC 3001, Australia
e-mail: raj.das@rmit.edu.au

Metamaterial With Local Resonators Coupled by Negative Stiffness Springs for Enhanced Vibration Suppression

In recent years, metamaterials for the applications in low-frequency vibration suppression and noise reduction have attracted numerous research interests. This paper proposes a metamaterial system with local resonators from adjunct unit cells coupled by negative stiffness springs. Frist, a lumped parameter model of the system is developed, and a stability criterion is derived. The band structure of the infinite lattice model is calculated. The result reveals the appearance of extra band gaps in the proposed metamaterial. A parametric study shows that the first extra band gap can be tuned to ultralow frequency by controlling the negative stiffness of the coupling springs. A transmittance analysis of the finite lattice model verifies the predictions obtained from the band structure analysis. Subsequently, the work is extended to a distributed parameter metamaterial beam model with the proposed configuration of coupled local resonators. The stability analysis shows that the infinitely long metamaterial beam becomes unstable as long as the stiffness of the coupling spring becomes negative. For the finitely long metamaterial beam, the stability could be achieved for negative coupling springs of given stiffnesses. The effects of the number of cells and the lattice constant on the system stability are investigated. The transmittance of the finitely long metamaterial beam is calculated. The result shows that due to the restriction on the tunability of negative stiffness for the proposed metamaterial beam, a quasistatic vibration suppression region can only be achieved when the number of cells is small.
[DOI: 10.1115/1.4043827]

1 Introduction

The suppression of structural vibrations is of great importance in engineering fields, including civil, automotive, aerospace, etc. Numerous passive [1–3] and active [4,5] methods have been proposed to deal with this problem over the past few decades. Utilizing periodic structures to form Bragg-scattering-type band gap is one of the technologies that has been proposed for vibration protection applications [6,7]. Specifically, engineered materials with periodic features are termed as phononic crystals. The key feature of this passive technique is the introduction of periodic impedance mismatch in the structures [8]. By employing the piezoelectric elements commonly used in the field of active vibration isolation, some researchers proposed active phononic crystals with tunable band gaps [9,10]. The main limitation of phononic crystals is that the band gap depends on the periodic spacing constant. The generation of low-frequency band gaps requires the periodic spacing constant to be designed in the same order of the wavelength of the low-frequency wave [11]. Due to the inverse relationship between the frequency and the wavelength, phononic crystals are not suitable for low-frequency vibration suppression applications.

The locally resonant metamaterial is a relatively new concept of a periodic structure that can also generate the band gap phenomenon. The work by Liu et al. [12] is deemed as the first realization of the locally resonant metamaterial. The underlying mechanism of generating band gap in the metamaterial is that the out-of-phase motions of the local resonators counteract the external excitation exerted on the main structure. The mass-in-mass model adopted in the research [13] helps understand the dynamic behavior of metamaterials including the negative effective mass concept which is closely related to the band gap. Metamaterials can overcome the limitation of the phononic crystals and generate low-frequency band gaps regardless of the periodic spacing constant. Therefore, the research on metamaterials has attracted extensive attention in recent years. An experimental study revealed the negative effect mass phenomenon in the mass-in-mass like structure [14]. Liu et al. [15] presented a theoretical study on the calculation of the band structure of a metamaterial beam with local resonators. Zhu et al. [16] proposed a metamaterial beam containing several different types of local resonators with different natural frequencies for broadband vibration suppression. Nouh et al. [17] designed a metamaterial plate with periodic local resonance structures. Huang and Sun [18] demonstrated a metamaterial consisting of multiresonator mass-in-mass lattice with multiple band gaps. Based on a different principle, Hu et al. [19] also proposed a metamaterial with multiple band gaps in the form of mass-in-mass lattice with internal couplings. Apart from various means to create multiple band gaps in metamaterials, the use of piezoelectric elements in metamaterials to achieve band gap tunability is also a way to achieve broad band gap. Chen et al. [20] introduced piezoelectric shunting arrays into sandwich plates. The resonance in the electrical circuit aroused the generation of the band gap which was tunable through the control of the electrical circuit. Zhu et al. [21] realized an adaptive metamaterial with controllable band gap through the tuning of the piezoelectric shunting circuit. Several other related researches in this direction were reported in

[1]Corresponding author.

Contributed by the Applied Mechanics Division of ASME for publication in the Journal of Applied Mechanics. Manuscript received March 18, 2019; final manuscript received May 20, 2019; published online June 4, 2019. Assoc. Editor: Haleh Ardebili.

Refs. [22–25]. In summary, in a variety of proposed metamaterials in the aforementioned researches, low-frequency band gaps range from tens to hundreds of Hz.

Although the low-frequency band gap phenomenon of metamaterials has already been extensively exploited, achieving ultralow/quasistatic frequency band gap (covering the frequency down to almost 0 Hz) is still a challenge. On this topic, Yu et al. [26] studied the wave propagation in a beam on elastic foundations. It is found that when the beam is attached with periodic local resonators, a very low-frequency vibration attenuation region could be generated for prohibiting the propagation of low-frequency waves. Lee et al. [27] fabricated an acoustic metamaterial tube with an array of side holes. Experimental results showed that sound below 450 Hz could not pass through the tube. Oh and Assouar [28] conceptually designed a metamaterial with zero rotational stiffness which has been analytically and numerically proved to be able to generate a quasistatic band gap, i.e., the band gap starts from almost 0 Hz. Drugan [29] presented a mathematical study of a periodic structure with stabilized negative stiffness components. It has been analytically predicted that the system can prohibit the propagation of long-wavelength waves which actually indicated the generation of an ultralow frequency band gap in the system. To the authors' best knowledge, very limited research has been conducted for achieving ultralow frequency (quasistatic) band gaps, which remains an extremely difficult but important engineering problem to date.

In this paper, a metamaterial system with local resonators coupled by negative stiffness springs is proposed for generating ultralow frequency band gap. The paper is organized as follows. Section 2 presents the analysis of a lumped parameter model of the proposed metamaterial. The stabilities of the finite and infinite lattice models are investigated. The criterion for ensuring the system stability is derived. Within the stabilized regime, the band structure of the infinite lattice model is analyzed. The result shows that the introduction of the negative stiffness springs makes the proposed metamaterial generate three band gaps. A parametric study reveals the possibility of the generation of the quasistatic band gap in the proposed metamaterial by tuning the negative stiffness of the coupling springs. The transmittance analysis of the corresponding finite lattice model is then performed to verify the predictions from the band structure analysis of the infinite lattice model. In Sec. 3, the study is extended to a metamaterial beam with the proposed configuration of local resonators. The finite element (FE) method is used to model the proposed metamaterial beam system. The mesh convergence is first performed to ensure the convergence of the models. The stabilities of the proposed metamaterial beams in both finitely and infinitely long forms are then investigated. The results show that the infinitely long metamaterial beam cannot include the proposed configuration, i.e., local resonators alternately coupled by negative stiffness springs. Only the stability criterion for the finitely long metamaterial beam model is given. The transmittance of the finitely long metamaterial beam is studied, and its dynamic behavior is discussed. Section 4 gives a brief discussion on the possible implementation of the negative stiffness coupling. Section 5 summarizes the main findings from this work.

2 Lumped Parameter Model

The mass-in-mass model has been widely employed for the investigation of metamaterials. The mathematical treatment of the lumped parameter model reflects the intrinsic mechanism of metamaterials. In this section, the focus is on the development of the proposed metamaterial with lumped parameters and evaluation of its band gap behavior.

2.1 Model Description. The lumped parameter model of the proposed metamaterial system is shown in Fig. 1. The unit cell of the system consists of two identical mass-in-mass structures connected in series. The outer and the inner masses of the mass-in-mass system are denoted by m_1 and m_2, respectively. The neighboring outer masses interact with each other via a spring of stiffness k_1. The inner and the outer masses within a unit cell are connected by a spring of stiffness k_2. The two inner masses m_2 are coupled by a spring of negative stiffness k_3. It should be noted that the negative stiffness spring only exists in the unit cell and couples the motions of the two inner masses in the unit cell. There is no negative spring between inner masses in neighboring unit cells.

Figures 1(*a*) and 1(*b*) show the infinite lattice model with the periodic boundary condition and the finite lattice model with the fixed (left) and free (right) boundary conditions.

For the infinite lattice model, the governing equations can be written as

$$\begin{cases} m_1\ddot{u}_1^{(2i+1)} + k_1(2u_1^{(2i+1)} - u_1^{(2i)} - u_1^{(2i+2)}) + k_2(u_1^{(2i+1)} - u_2^{(2i+1)}) = 0 \\ m_2\ddot{u}_2^{(2i+1)} + k_2(u_2^{(2i+1)} - u_1^{(2i+1)}) + k_3(u_2^{(2i+1)} - u_2^{(2i+2)}) = 0 \\ m_1\ddot{u}_1^{(2i+2)} + k_1(2u_1^{(2i+2)} - u_1^{(2i+1)} - u_1^{(2i+3)}) + k_2(u_1^{(2i+2)} - u_2^{(2i+2)}) = 0 \\ m_2\ddot{u}_2^{(2i+2)} + k_2(u_2^{(2i+2)} - u_1^{(2i+2)}) + k_3(u_2^{(2i+2)} - u_2^{(2i+1)}) = 0 \end{cases} \tag{1}$$

where $u_1^{(k)}$ and $u_2^{(k)}$ denote the displacements of the outer and inner masses in the kth mass-in-mass structure, respectively. Each unit cell is formed by two mass-in-mass structures. The superscripts, $k = 2i + 1$ and $2i + 2$, denote the two neighboring mass-in-mass structures in the $(i + 1)$th unit cell.

For the finite lattice model consisting of n unit cells (i.e., $2n$ mass-in-mass structures), apart from the two unit cells at the boundaries, the governing equations of the inner unit cells are the same as

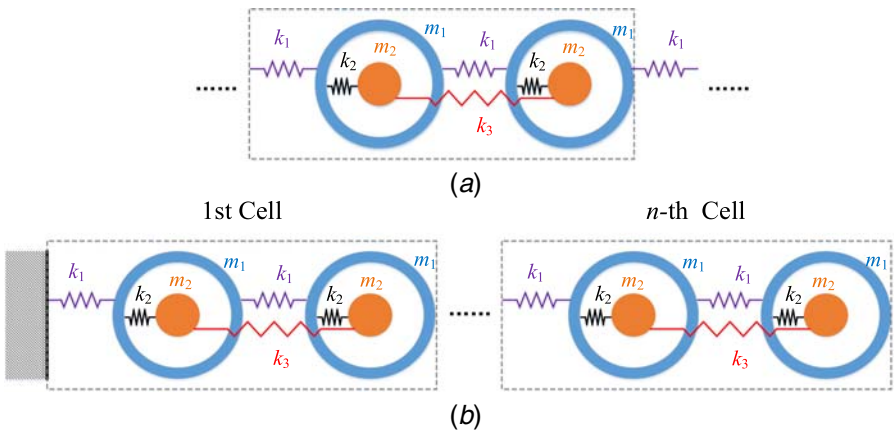

Fig. 1 (*a*) Infinite lattice model and (*b*) finite lattice model of the metamaterial with local resonators coupled by negative stiffness springs

Eq. (1). At the boundaries, the governing equations of the first and last outer masses are given separately as follows:

$$\begin{cases} m_1\ddot{u}_1^{(1)} + k_1(2u_1^{(1)} - u_0 - u_1^{(2)}) + k_2(u_1^{(1)} - u_2^{(1)}) = 0 \\ m_1\ddot{u}_1^{(2n)} + k_1(u_1^{(2n)} - u_1^{(2n-1)}) + k_2(u_1^{(2n)} - u_2^{(2n)}) = 0 \end{cases} \tag{2}$$

It can be anticipated that with an increase of the number of cells, the dynamic behavior of the finite lattice model should approach that of the infinite lattice model (except minor differences at the boundaries).

2.2 Stability Analysis. Since negative stiffness springs are introduced in the proposed metamaterial system, the proposed system is prone to lose stability. Before any further study is conducted, it is crucial to investigate the stability of this system first. As presented in Sec. 2.1, there are infinite and finite lattice models. Since the infinite lattice model can be regarded as an extreme case of the finite lattice model, we naturally embark on the finite lattice model. Then, with the increase in the number of cells to a large value, it is possible to derive the stability of the infinite lattice model.

2.2.1 Finite Lattice Model. For the stability of the linear systems, it can be judged according to the eigenvalues of Jacobi's matrix [30]. First, we rearrange the governing equations of the finite lattice model in the first order form

$$\dot{\boldsymbol{x}} = \boldsymbol{X}(\boldsymbol{x}) \tag{3}$$

where $\boldsymbol{x} = \left[u_1^{(1)} \;\; \dot{u}_1^{(1)} \;\; u_2^{(1)} \;\; \dot{u}_2^{(1)} \;\; u_1^{(2)} \;\; \dot{u}_1^{(2)} \;\; u_2^{(2)} \;\; \dot{u}_2^{(2)} \;\; \cdots \;\; u_1^{(2i+1)} \;\; \dot{u}_1^{(2i+1)} \;\; u_2^{(2i+1)} \;\; \dot{u}_2^{(2i+1)} \;\; u_1^{(2i+2)} \;\; \dot{u}_1^{(2i+2)} \;\; u_2^{(2i+2)} \;\; \dot{u}_2^{(2i+2)} \;\; \cdots \right]$.

Jacobi's matrix $\boldsymbol{A}$ is thus obtained as

$$\boldsymbol{A} = (a_{rk})_N \quad \text{and} \quad a_{rk} = \left(\frac{\partial X_r}{\partial x_k} \right)_{x_k = 0} \tag{4}$$

It is noteworthy that $\boldsymbol{A}$ is a $N \times N$ square matrix and $N = 8n$, a_{rk} is the rth row and kth column element of matrix $\boldsymbol{A}$. If the real parts of all the eigenvalues λ of $\boldsymbol{A}$ are negative, i.e., $\mathrm{Re}(\lambda) < 0$, then the response of the system must be asymptotically stable for $t \to \infty$. Otherwise, if there exists an eigenvalue λ of $\boldsymbol{A}$ with a positive real part, i.e., $\mathrm{Re}(\lambda) > 0$, then the response of the system must be unstable for $t \to \infty$.

2.2.2 Infinite Lattice Model. Regarding the stability of the infinite lattice model, it is not convenient to directly apply the same method by checking the eigenvalues of Jacobi's matrix. Starting from the infinite lattice assumption, i.e., the periodic boundary condition, by applying Bloch's theorem, one can express the wave form of the harmonic displacements of the outer and inner masses in the $(2i+1)$th and $(2i+2)$th mass-in-mass structures as

$$\begin{cases} u_1^{(2i+1)} = Ae^{j(qx-\omega t)} \\ u_1^{(2i+2)} = Be^{j(qx+qL-\omega t)} \\ u_2^{(2i+1)} = Ce^{j(qx-\omega t)} \\ u_2^{(2i+2)} = De^{j(qx+qL-\omega t)} \end{cases} \tag{5}$$

where q is the wave number. A, B, C, and D are the complex wave amplitudes. Substituting Eq. (5) into Eq. (1) yields

$$\begin{bmatrix} 2k_1 + k_2 - m_1\omega^2 & -2k_1\cos(qL) & -k_2 & 0 \\ -k_2 & 0 & k_2 + k_3 - m_2\omega^2 & -k_3e^{jqL} \\ -2k_1\cos(qL) & 2k_1 + k_2 - m_1\omega^2 & 0 & -k_2 \\ 0 & -k_2 & -k_3e^{-jqL} & k_2 + k_3 - m_2\omega^2 \end{bmatrix} \begin{bmatrix} A \\ B \\ C \\ D \end{bmatrix} = \begin{bmatrix} 0 \\ 0 \\ 0 \\ 0 \end{bmatrix} \tag{6}$$

where L is the lattice constant. To ensure the existence of nontrivial solutions of A, B, C, and D, the determinant of the coefficient matrix of Eq. (6) needs to be zero. This condition states the dispersion relation between the wavenumber of the wave propagated in the metamaterial and its frequency. By sweeping the wavenumber, the corresponding frequencies can be obtained. For a stable system, for any wavenumber, the corresponding wave frequencies must be real values. On the other hand, for an unstable system, there will be solutions of wave frequencies with negative imaginary parts for any wavenumber. This indicates that the response of the system grows to infinity (i.e., unstable) for $t \to \infty$. It is worth noting that the underlying principles of both methods, i.e., evaluating eigenvalues of Jacobi's matrix and calculating the wave frequencies, are actually the same. The eigenvalues contain information about the properties of the wave solutions. In order to make the results of the subsequent study more general, several dimensionless parameters are introduced.

$$\mu = \frac{m_2}{m_1}; \quad \alpha = \frac{\omega_1}{\omega_2}; \quad \beta = \frac{k_3}{k_2} \tag{7}$$

where $\omega_1 = \sqrt{k_1/m_1}$ and $\omega_2 = \sqrt{k_2/m_2}$.

By using the aforementioned methods, the criteria for ensuring the stability of both the finite and infinite lattice models are derived. Figure 2 shows the dimensionless critical negative stiffness, i.e., critical β_c for the system with respect to μ and α. The critical value of β_c means that if $\beta \geq \beta_c$, the system is stable; otherwise, the system is unstable. It is worth mentioning that Fig. 2 represents the results for both finite and infinite lattice models. Moreover, for the finite lattice model, regardless of the number of cells that the system contains, the critical β_c is always the same for given μ and α. Therefore, it can be stated that the stability conditions of both the finite and infinite lattice models should be the same as that of the unit cell. In other words, the stability condition of the system only depends on the stability condition of the unit cell that constitutes the system. The following investigations are conducted based on the prerequisite that the system stability is ensured, i.e., restricting β in the stable regime ($\beta \geq \beta_c$).

2.3 Negative Effective Mass. One of the most important features of metamaterials is that the effective mass could become

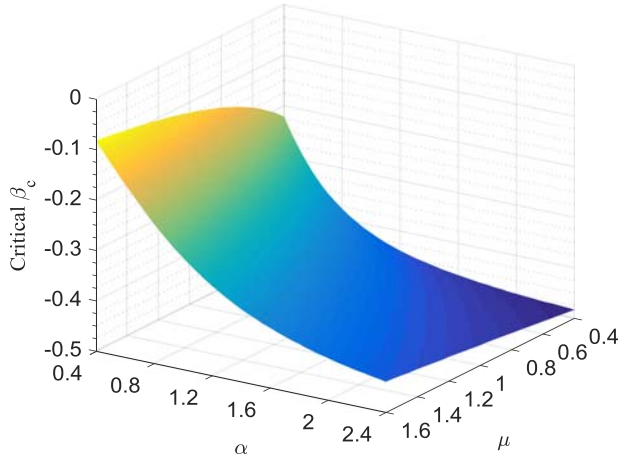

Fig. 2 Critical β_c versus μ and α

negative within a certain range of frequency [14]. Moreover, the negative effective mass characteristic is closely related to the band gap phenomenon. Therefore, within the stable regime, this section investigates the effective mass of the proposed metamaterial.

The basic unit cell of the proposed metamaterial is shown in Fig. 1(*a*). By assuming that the internal interactions within the unit cell are all absorbed by the left-hand side outer mass m_1, one can use an effective mass m_{eff} to represent the unit cell. Considering Newton's second law, the acceleration of an object is directly proportional to the force applied on it and inversely proportional to its mass. To calculate the effective mass, one can assume that a harmonic force is directly exerted on the left-hand side outer mass in a given unit cell. Through the manipulation of the governing equations of the unit cell, the displacements of other masses can be eliminated except the displacement of the left-hand side outer mass. The relationship between the displacement of the left-hand side outer mass and the force is then obtained. Since the applied force is assumed to be in the harmonic form, the displacement and acceleration responses should also be in the harmonic form. Therefore, based on the obtained relationship between the force and the displacement of the left-hand side outer mass, the effective mass m_{eff} can be obtained

$$\frac{m_{\text{eff}}}{m_1} = \frac{\Omega^6 - 2(\alpha^2+\beta+\mu+1)\Omega^4 + [2\alpha^2(2\beta+\mu+2)+\mu(4\beta+\mu)+2(\beta+\mu)+1]\Omega^2 - 2(\mu+1)[\alpha^2(2\beta+1)+\beta\mu]}{\Omega^6 - (\alpha^2+2\beta+\mu+2)\Omega^4 + [2\alpha^2(\beta+1)+(2\beta+1)(\mu+1)]\Omega^2 - [\alpha^2(2\beta+1)+\beta\mu]} \tag{8}$$

It can be noted that the effective mass m_{eff} is frequency dependent. For given $\mu = 0.4$ and $\alpha = 1.2$, the dimensionless effective mass m_{eff}/m_1 is plotted against the dimensionless frequency Ω ($\Omega = \omega/\omega_2$) as shown in Fig. 3. The result of the conventional metamaterial without negative spring interaction (i.e., $\beta = 0$) is included for comparison. From the knowledge of the conventional metamaterial, the band gap appears around the frequency range where the effective mass becomes negative. As shown in Fig. 3, the effective mass of the conventional metamaterial always becomes negative around $\Omega = 1$. For the proposed metamaterial (i.e., $\beta \neq 0$), the effective mass becomes negative for three times in three different frequency ranges (for $\Omega < 1$, slightly less than $\Omega = 1$, and for $\Omega > 1$). It is noted that the frequency where the negative effective mass m_{eff} appears for the first time in $\Omega < 1$ varies significantly with the increase of the magnitude of β. While the frequencies at which negative m_{eff} appears for the second and third times have small variation with respect to β.

2.4 Band Structure Analysis. This section investigates the band gap behavior of the proposed metamaterial based on the infinite lattice model. Although the infinite lattice model theoretically has infinite number of degrees of freedom (DOFs), the periodic boundary condition derived from the infinite assumption actually significantly simplifies the complexity of this problem. Therefore, the infinite lattice model will be treated first to give a prediction of the dynamic characteristics of the proposed metamaterial system. The finite lattice model will then be solved to confirm the prediction from the infinite lattice model.

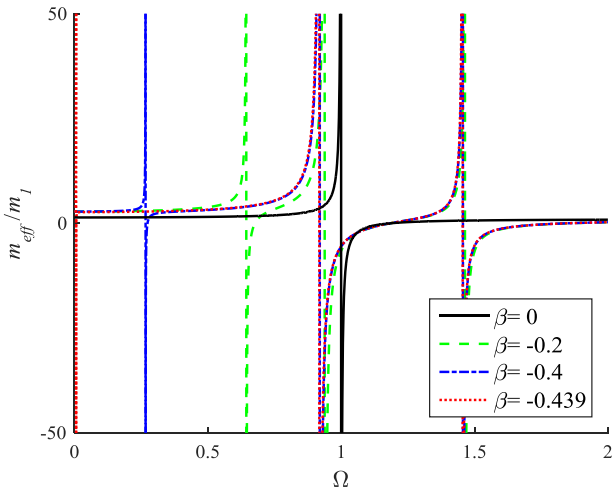

Fig. 3 Dimensionless effective mass m_{eff}/m_1 versus dimensionless frequency Ω

By directly using Bloch's theorem to describe the periodic boundary conditions and then forcing the determinant of the coefficient matrix of Eq. (6) to be zero, one could obtain the dispersion relation of the proposed metamaterial. However, the result of this technique does not provide information regarding attenuation apart from the band gap ranges. The transfer matrix method is therefore utilized for the band structure analysis of the proposed metamaterial. The implementation of the transfer matrix method mainly relies on the formulation of the transfer matrix of the lattice that relates the forces and displacements at the left and right cell boundaries (Fig. 4).

f_L and f_I are the forces exerted on the left and right outer masses in one unit cell from their left-hand sides, respectively. u_L and u_I are their displacements. f_R and u_R are the corresponding force and displacement related to the left outer mass of the succeeding unit cell. x_L and x_I are the displacements of the left and right inner masses, respectively. By adhering to the notations shown in Fig. 4, the governing equations of the left-hand side mass-in-mass system can be written as

$$\begin{cases} -m_1\omega^2 U_L + k_1(U_L - U_I) + k_2(U_L - X_L) = -F_L \\ -m_2\omega^2 X_L + k_2(X_L - U_L) + k_3(X_L - X_I) = 0 \\ F_I = k_1(U_I - U_L) \end{cases} \tag{9}$$

The capitalized symbols in Eq. (9) represent the corresponding amplitudes (e.g., U_L is the amplitude of u_L). Similarly, the governing equations of the right-hand side mass-in-mass system are expressed as

$$\begin{cases} -m_1\omega^2 U_I + k_1(U_I - U_R) + k_2(U_I - X_I) = -F_I \\ -m_2\omega^2 X_I + k_2(X_I - U_I) + k_3(X_I - X_L) = 0 \\ F_R = k_1(U_R - U_I) \end{cases} \tag{10}$$

Combining the second equation of Eq. (9) and the second equation of Eq. (10), one could solve for X_L and X_I in terms of U_L and U_I. Subsequently, substituting the expression of X_L into the first equation of Eq. (9) and in conjunction with the third equation of Eq. (9),

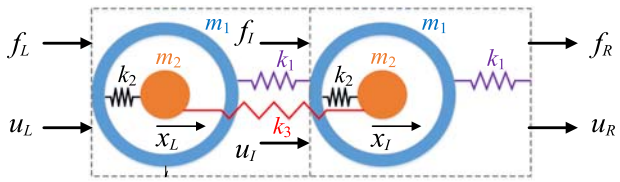

Fig. 4 Force and displacement interactions at the interfaces

one could express F_I and U_I in terms of F_L and U_L as follows:

$$\begin{bmatrix} F_I \\ U_I \end{bmatrix} = \begin{bmatrix} B_{11} & B_{12} \\ B_{21} & B_{22} \end{bmatrix} \begin{bmatrix} F_L \\ U_L \end{bmatrix} \tag{11}$$

where

$$B_{11} = \frac{k_1(m_2^2\omega^4 - 2(k_3+k_2)m_2\omega^2 + 2k_3k_2 + k_2^2)}{k_1m_2^2\omega^4 - 2k_1m_2(k_3+k_2)\omega^2 + 2k_3k_1k_2 + k_3k_2^2 + k_1k_2^2}$$

$$B_{12} = \frac{k_1(-m_1m_2^2\omega^6 + (2k_3m_1m_2 + 2k_2m_1m_2 + k_2m_2^2)\omega^4 - (2k_3k_2m_1 + 2k_3k_2m_2 - k_2^2m_1 - k_2^2m_2)\omega^2)}{k_1m_2^2\omega^4 - 2k_1m_2(k_3+k_2)\omega^2 + 2k_3k_1k_2 + k_3k_2^2 + k_1k_2^2}$$

$$B_{21} = \frac{m_2^2\omega^4 - 2m_2(k_3+k_2) + 2k_3k_2 + k_2^2}{k_1m_2^2\omega^4 - 2k_1m_2(k_3+k_2)\omega^2 + 2k_3k_1k_2 + Kk_2^2 + k_1k_2^2}$$

$$B_{22} = \frac{\begin{bmatrix} -m_1m_2^2\omega^6 + (2k_3m_1m_2 + k_1m_2^2 + 2k_2m_1m_2 + k_2m_2^2)\omega^4 \\ -(2k_3k_1m_2 + 2k_3k_2m_1 + 2k_3k_2m_2 + 2k_1k_2m_2 + k_2^2m_1 + k_2^2m_2)\omega^2 + 2k_3k_1k_2 + k_3k_2^2 + k_1k_2^2 \end{bmatrix}}{k_1m_2^2\omega^4 - 2k_1m_2(k_3+k_2)\omega^2 + 2k_3k_1k_2 + k_3k_2^2 + k_1k_2^2}$$

By following the same procedure, considering the right-hand side mass-in-mass system, F_R and U_R can be expressed in terms of F_I, U_I, F_L, and U_L as follows:

$$\begin{bmatrix} F_R \\ U_R \end{bmatrix} = \begin{bmatrix} C_{11} & C_{12} \\ C_{21} & C_{22} \end{bmatrix} \begin{bmatrix} F_I \\ U_I \end{bmatrix} + \begin{bmatrix} D_{11} & D_{12} \\ D_{21} & D_{22} \end{bmatrix} \begin{bmatrix} F_L \\ U_L \end{bmatrix} \tag{12}$$

where

$$C_{11} = 1$$

$$C_{12} = \frac{-m_1m_2^2\omega^6 + (2k_3m_1m_2 + 2k_2m_1m_2 + k_2m_2^2)\omega^4 - (2k_3k_2m_1 + 2k_3k_2m_2 + k_2^2m_1 + k_2^2m_2)\omega^2 + k_3k_2^2}{m_2^2\omega^4 - 2(k_3+k_2)m_2 + 2k_3k_2 + k_2^2}$$

$$C_{21} = \frac{1}{k_1}$$

$$C_{22} = \frac{\begin{bmatrix} -m_1m_2^2\omega^6 + (2k_3m_1m_2 + k_1m_2^2 + 2k_2m_1m_2 + k_2m_2^2)\omega^4 \\ -(2k_3k_1m_2 + 2k_3k_2m_1 + 2k_3k_2m_2 + 2k_1k_2m_2 + k_2^2m_1 + k_2^2m_2)\omega^2 \\ +2k_3k_1k_2 + k_3k_2^2 + k_1k_2^2 \end{bmatrix}}{k_1[m_2^2\omega^4 - 2(k_3+k_2)m_2 + 2k_3k_2 + k_2^2]}$$

$$D_{11} = 0$$

$$D_{12} = -\frac{k_3k_2^2}{m_2^2\omega^4 - 2(k_3+k_2)m_2 + 2k_3k_2 + k_2^2}$$

$$D_{21} = 0$$

$$D_{22} = -\frac{k_3k_2^2}{k_1[m_2^2\omega^4 - 2(k_3+k_2)m_2 + 2k_3k_2 + k_2^2]}$$

Through the manipulation of Eqs. (11) and (12) by eliminating F_I and U_I, one could derive the transfer matrix $\mathbf{T}$ that relates the forces and displacements at the left and right cell boundaries.

$$\begin{bmatrix} F_R \\ U_R \end{bmatrix} = \underbrace{\left\{ \begin{bmatrix} C_{11} & C_{12} \\ C_{21} & C_{22} \end{bmatrix} \begin{bmatrix} B_{11} & B_{12} \\ B_{21} & B_{22} \end{bmatrix}^{-1} + \begin{bmatrix} D_{11} & D_{12} \\ D_{21} & D_{22} \end{bmatrix} \right\}}_{\mathbf{T}} \begin{bmatrix} F_L \\ U_L \end{bmatrix} \tag{13}$$

According to the periodic boundary condition, by using Bloch's theorem, the forces and displacements at the left and right cell boundaries could be related in the form as

$$\begin{bmatrix} F_R \\ U_R \end{bmatrix} = \begin{bmatrix} e^{jqL} & 0 \\ 0 & e^{jqL} \end{bmatrix} \begin{bmatrix} F_L \\ U_L \end{bmatrix} \tag{14}$$

Comparing Eqs. (13) and (14) yields a standard eigenvalue problem of the transfer matrix $\mathbf{T}$.

$$|\mathbf{T} - e^{jqL}\mathbf{I}| = 0 \tag{15}$$

where $\mathbf{I}$ is the 2×2 unit matrix. For a given ω, solving Eq. (15) gives the solutions of q. The property of q contains the information that predicts the wave propagation behavior in the metamaterial. Imaginary q indicates an evanescent wave that will decay quickly with an increase in the propagation distance. This means that the corresponding wave frequency falls into the band gap.

Given $\mu = 0.4$ and $\alpha = 1.2$, Figs. 5 and 6 show the real and imaginary parts, respectively, of the complex band structures for the proposed metamaterials with different values of β. The x-axis and the y-axis denote the normalized wave number $q^* = qL/\pi$ and the dimensionless frequency $\Omega = \omega/\omega_2$, respectively. The case of the conventional metamaterial without the negative stiffness coupling springs is represented by $\beta = 0$ (Figs. 5(*a*) and 6(*a*)).

As seen in Figs. 5(*b*)–5(*d*), with the introduction of the negative stiffness coupling springs, there appear three band gaps in the proposed metamaterial. The second band gap of the proposed metamaterial is also located around $\Omega = 1$, like the band gap of the conventional metamaterial but becomes wider. From the point of view of only the second band gap, the proposed metamaterial is already superior to the conventional one due to this wider band gap. Moreover, the existence of the two additional band gaps is the further superiority of the proposed metamaterial in terms of the broadband vibration suppression. It is noted that with the increase of the magnitude of β, the first band gap of the proposed metamaterial becomes wider and moves downward to the lower frequency. While the second and the third band gaps are not very sensitive to the change of β, it is worth mentioning that Fig. 5(*d*) presents the result corresponding to the critical value, $\beta_c = -0.439$, of this example system. One can note that by tuning to the critical β_c, we are able to achieve an ultralow frequency (almost quasistatic) band gap. It is to note that the limitation of Bragg scattering phononic crystals is the difficulty in their usage effectively in low-frequency applications, and one main advantage of the locally resonant metamaterials is the ease design that allows achieving low-frequency band gaps. Therefore, from the point of view of the generation of the quasistatic band gap, the proposed metamaterial demonstrates the superiority in ultralow frequency wave manipulation.

To inspect the attenuation abilities of the band gaps, Fig. 6 shows the corresponding imaginary parts of the complex band structures of the proposed metamaterials. The larger the imaginary part is, the more rapidly the wave decays with the increase of the propagation distance, i.e., the better the attenuation ability is. It can be observed that in terms of the magnitude of the imaginary part, the conventional metamaterial (Fig. 6(*a*)) exhibits the best attenuation capacity. However, because the second band gap of the proposed metamaterial is not much smaller than that of the conventional one, and the attenuation and the imaginary magnitude are exponentially related, the imaginary part of the proposed metamaterial is of the same order of attenuation. Therefore, the width of the band gap is more important. In addition, it can be noted that the imaginary part of the third band gap is very small, and it is thus expected that its attenuation ability is considerably weak for practical use in finite lattice models. Besides, one can find that the magnitude

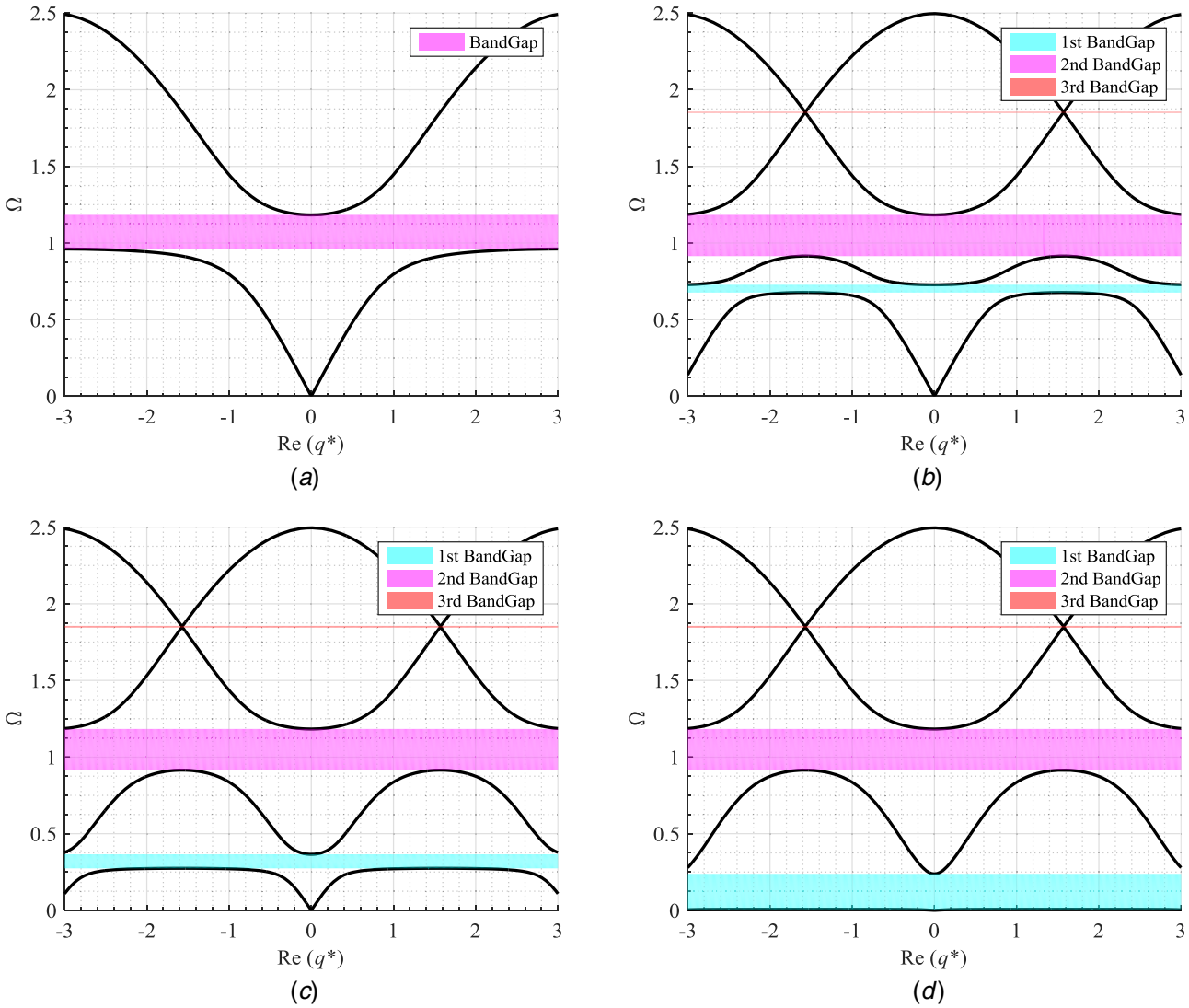

Fig. 5 Real part of complex band structures of the proposed metamaterial with different β: (*a*) $\beta = 0$ (i.e., the conventional metamaterial), (*b*) $\beta = -0.2$, (*c*) $\beta = -0.4$, and (*d*) $\beta = -0.439$

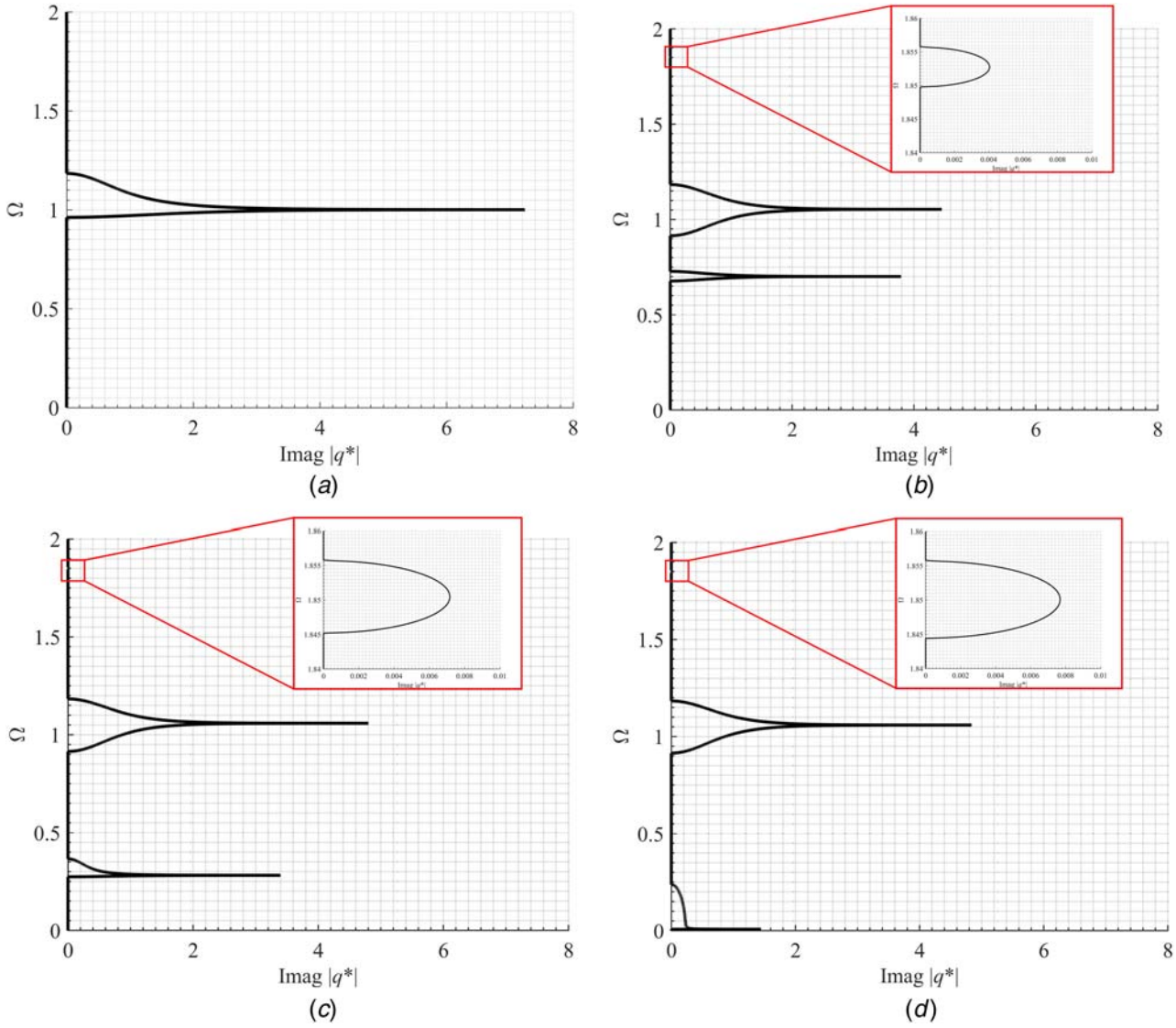

Fig. 6 Imaginary part of complex band structures of the proposed metamaterial with different values of β: (a) $\beta = 0$ (i.e., the conventional metamaterial), (b) $\beta = -0.2$, (c) $\beta = -0.4$, and (d) $\beta = -0.439$

of the imaginary part of the first band gap decreases with the increase of the magnitude of β. This indicates that though one may create a quasistatic band gap by tuning β to approach the critical value β_c, the practical vibration suppression ability of the first band gap in the finite lattice model with only limited number of cells may not be that satisfactory. However, this does not mean that the quasistatic band gap is meaningless. To ensure the quasistatic band gap to take an obvious effect, one could increase the number of cells of the finite lattice model. This point will be demonstrated and proved in Sec. 2.5.

To understand the effects of β on the band gap behavior of the proposed metamaterial, thus providing some guidelines to tune β for the potential optimized design, a parametric study is conducted. Figure 7 shows the evolution of the band gaps of the proposed metamaterials with the variation of β, with μ and α being kept unchanged with values of $\mu = 0.4$ and $\alpha = 1.2$. β varies from 0 to $\beta_c = -0.439$. It can be found that as long as $\beta \neq 0$, there appears two additional band gaps. With an increase in the magnitude of β (i.e., the increase in the strength of the negative coupling spring), the original band gap (i.e., the second band gap) first becomes wider and then remains almost unchanged ($\beta < -0.044$). The widths of the first and third band gaps increase monotonically. However, even when β is tuned

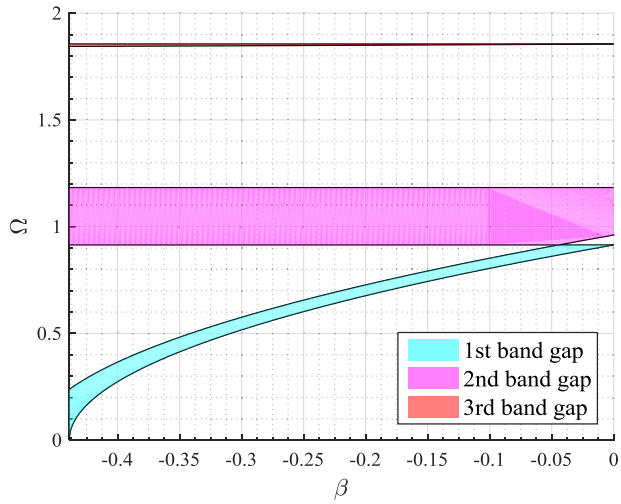

Fig. 7 Evolution of band gaps of the proposed metamaterial with varying β

to β_c, the actual width of the third band gap is still very narrow. The width of the first band gap is also narrow when β is near 0; however, when β is tuned to β_c, its width increases and becomes comparable with the second band gap. In addition, it is worth mentioning that when β is tuned around -0.044, the first and second band gaps merge together.

Since the previous results show that the proposed metamaterial at critical β_c exhibits an extraordinary phenomenon, i.e., the first band gap becomes a quasistatic band gap, naturally, one will query whether this phenomenon exists only in the special case (i.e., when $\mu = 0.4$ and $\alpha = 1.2$) or it exists with arbitrary values of μ and α. To answer this question, the evolution of the band gaps of the proposed metamaterials at critical β_c with varying μ and α is shown in Fig. 8.

It can be seen that regardless of the variation of the system in terms of μ and α, the quasistatic band gap could always be achieved at the critical value of β_c. Moreover, one can observe the evolution trends of band gaps with the variation of μ and α. With an increase in μ and decrease in α, the widths of the first and the second band gaps increase. However, the third band gap is always very narrow. Nevertheless, the benefits from the appearance of the first additional band gap and the enhancement of the second band gap have already ensured the superiority of the proposed metamaterial.

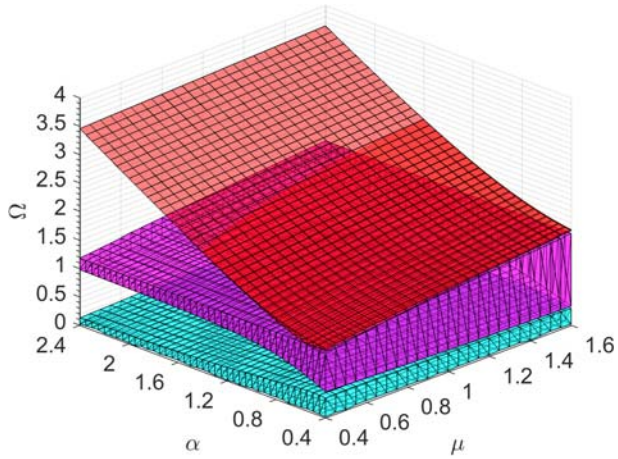

Fig. 8 Evolution of the band gaps of the proposed metamaterials at critical β_c with varying μ and α

2.5 Transmittance Analysis. Real systems cannot be infinitely long. In practical applications, metamaterials are constituted of limited number of cells. In this section, investigations on the finite lattice model of the proposed metamaterial are conducted to verify the predictions from the band structure analysis based on the infinite lattice model. The performance of the proposed metamaterial consisting of limited number of cells is examined. A similar metamaterial system but with positive stiffness coupling springs has already been reported in Ref. [19]. The mathematical modeling procedure is the same as Ref. [19]. Therefore, the detailed procedure is not repeated here.

Figure 9(*a*) presents the transmittances of the proposed metamaterial consisting of limited cells with different β. μ and α are kept the same with values $\mu = 0.4$ and $\alpha = 1.2$. It is worth noting that $\beta = 0$ represents the case of the conventional metamaterial. For the cases of $\beta \neq 0$, the finite lattice models consist of 5 cells, i.e., 10 mass-in-mass structures as one unit cell contains 2 mass-in-mass structures. For the case of $\beta = 0$, the finite lattice consist of 10 cells, i.e., 10 mass-in-mass structures, since each cell contains 1 mass-in-mass structure. Hence, it is a fair comparison between the proposed and conventional metamaterials. As expected, there is only one vibration attenuation region in the transmittance of the conventional metamaterial. For the cases when $\beta \neq 0$, there appears two vibration attenuation regions in the transmittance. These two vibration attenuation regions correspond to the first two band gaps predicted from the band structure analysis (Fig. 5). As discussed previously, since the attenuation of the third band gap is very weak, in the finite lattice model consisting of only limited number of cells, it does not show up as an effective vibration attenuation region.

Regarding the second vibration suppression region, it is found in Fig. 9 that its width is larger than that of the conventional one (i.e., $\beta = 0$), which is consistent with what was obtained in the band structure analysis (Fig. 5). Moreover, regardless of the change of β excepting $\beta = 0$, the width of the second vibration attenuation region is almost unaffected, which is also consistent with the prediction from the band structure analysis (Fig. 7). In terms of the first vibration suppression region, one can find that with the increase of the magnitude of β, its width becomes larger and it moves toward the lower frequency. At $\beta = \beta_c$, the first vibration attenuation region starts almost from 0 Hz which is in accordance with the predicted quasistatic band gap phenomenon. In addition, it is observed that with an increase in the magnitude of β, the trough of the first vibration attenuation region becomes shallower which indicates a reduction in the attenuation ability. This also confirms the result obtained from the analysis of the imaginary part of the complex band structure (Fig. 6).

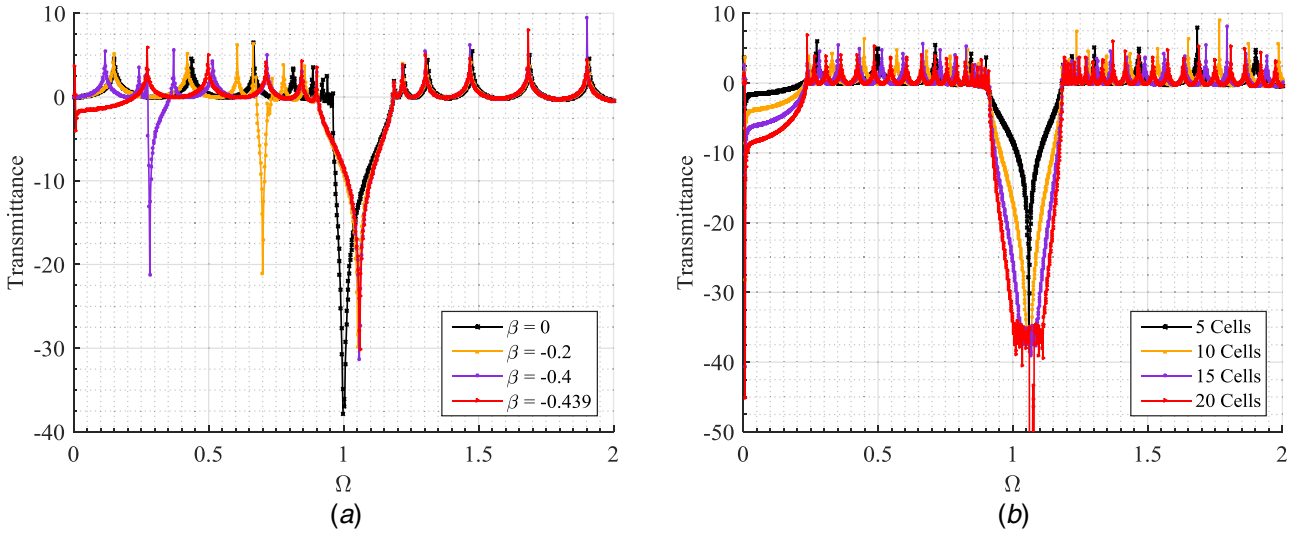

Fig. 9 Transmittances of the finite lattice model of the proposed metamaterial consisting of (*a*) five cells with different values of β and (*b*) different number of cells at critical β_c

Due to this fact, though a quasistatic vibration suppression region is generated, its practical vibration suppression capability is not as effective as that of the second vibration suppression region. To address this issue, one may increase the number of cells to deepen the first vibration suppression region.

Figure 9(*b*) shows the transmittances of the proposed metamaterial by increasing the number of cells. As already expected, with an increase in the number of cells, the vibration suppression ability of the first attenuation region is significantly enhanced. Therefore, it can be concluded that by carefully tuning the system parameters, the proposed metamaterial with negative stiffness coupling springs could provide a way to achieve ultralow frequency vibration suppression, which will lead to their usages in many important applications.

3 Distributed Parameter Model

The beam is a structural element that is widely used in practical engineering. The concept of metamaterials in the design of beams can be adopted for suppressing vibrations. In this section, we propose a metamaterial beam with local resonators coupled by negative stiffness springs.

3.1 Model Description. The schematic of the proposed metamaterial beam with local resonators coupled by negative stiffness springs is shown in Fig. 10. Figures 10(*a*) and 10(*b*) show the infinitely long and finitely long metamaterial beam models, respectively. The thickness and width of the beam are h_s and b, respectively. The mass density and Young's modulus of the material that constitute the host beam are ρ and E_s, respectively. Uniform local resonators are periodically attached onto the host beam at a constant spacing of d, i.e., the lattice constant. These are modeled as lumped mass-spring systems with the mass denoted by m_2 and the stiffness denoted by k_2. The neighboring two local resonators are alternately coupled by a negative stiffness coupling spring k_3. To calculate the band structure of the infinitely long model, one could apply the most widely used transfer matrix method. For the transmittance of the finitely long metamaterial beam, either the transfer matrix method or an approximate analytical method [31] could be employed. However, considering the convenience for the later study of system stability, the finite element method proposed in Ref. [32] is adopted for developing the model of the proposed metamaterial beam.

The host beam is discretised with the one-dimensional two-node finite element. Each node of the discretised element has two DOFs: translation u and rotation θ. The explicit expressions of the element mass and stiffness matrices can be referred to Ref. [32]. After the assembly of the element matrices, the global matrices and the global governing equations of motion can then be obtained as

$$\mathbf{M}\ddot{\mathbf{u}} + \mathbf{K}\mathbf{u} = \mathbf{F} \tag{16}$$

For the infinitely long model, it is only required to build the governing equations of a unit cell and the right-hand side force term $\mathbf{F}$ is dropped, since the band structure analysis is conducted under the assumption of free vibration. The periodic boundary condition can then be translated by using Bloch's theorem. The amplitudes of the displacements and rotations of the nodes at the left-hand side (i.e., $[u_R \quad \theta_R]^T$) and right-hand side (i.e., $[u_R \quad \theta_R]^T$) cell boundaries are related as

$$\begin{bmatrix} u_R \\ \theta_R \end{bmatrix} = e^{jqd} \begin{bmatrix} u_L \\ \theta_L \end{bmatrix} \tag{17}$$

For the finitely long model, the mathematical treatment of the clamped boundary condition is by eliminating the first two rows and columns in the global mass and stiffness matrices. The translation and rotation DOFs of the first node are completely constrained to be zero. The physically clamped boundary condition is thus mathematically implemented. The detailed finite element formulation is similar to that for a metamaterial beam without coupling springs k_3 which can be found in Ref. [32] and thus is not repeated here.

3.2 Convergence Study. The finite element method is selected for performing the study of the proposed metamaterial beam. The mesh convergence is an important issue in the accuracy of the finite element method. Therefore, to ensure the mesh is fine enough and produces converged results, a mesh convergence analysis is first undertaken. Taking a cantilevered plain beam as an example and considering its transverse vibration, the convergence of the model is investigated by increasing the mesh density

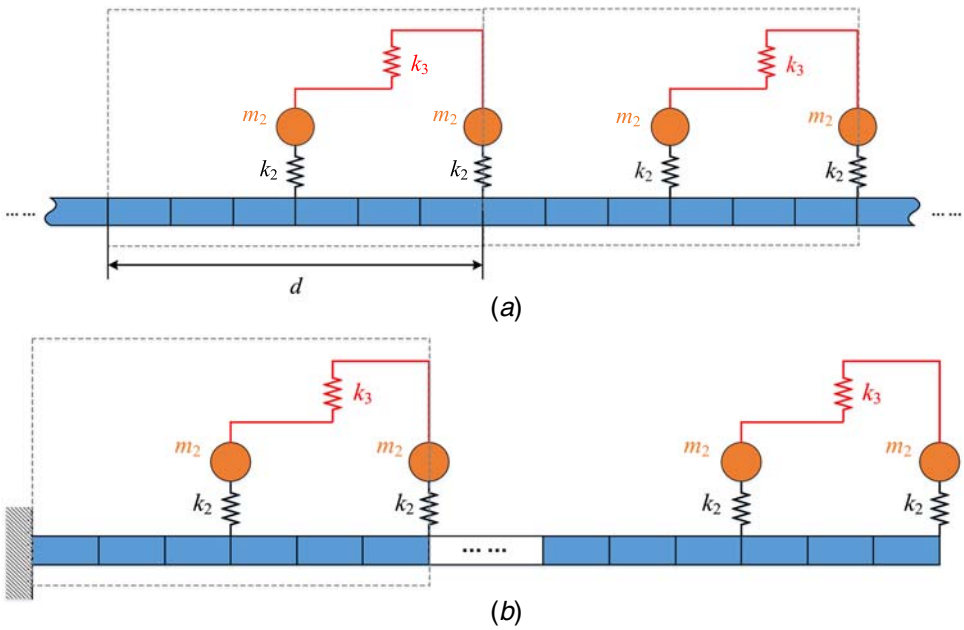

Fig. 10 (*a*) Infinitely long model and (*b*) finitely long model of the proposed metamaterial beam with local resonators coupled by negative stiffness springs. The host beam is discretised as finite elements.

Table 1 Geometric and material parameters of the cantilevered plain beam

Parameters	Values
Beam length, L	500 mm
Beam width, b	20 m
Beam thickness, h_s	4 mm
Beam density, ρ	7850 kg/m^3
Young's modulus of the beam, E_s	200 GPa

(i.e., number of elements). The geometric and material parameters of the plain beam under investigation are listed in Table 1.

The variation of the calculated first four natural frequencies of the cantilevered plain beam with the change of the mesh density is presented in Fig. 11. The corresponding finite element model is also created with the commercial software ANSYS for verification and to use as the reference solution for the mesh convergence study. The results of the first four natural frequencies from ANSYS are 13.046, 81.735, 228.767, and 448.029 Hz, respectively. It can be seen that the calculated natural frequencies converge with an increase in the mesh density. The converged values agree well with those predicted by the ANSYS, but there is still a bit difference. The error of the FE method increases for predicting higher order of natural frequencies. However, since within the frequency range of interest, the error is very minor. It is deemed that the results from the employed FE method are authentic. It is worth mentioning that when the entire beam is meshed with 20 elements, the corresponding element length is 25 mm. From the point of view of the meshed element length, this indicates that for a beam of the same material, width and thickness, by dividing it into elements with a length less than 25 mm, the convergence of the model can be guaranteed.

3.3 Stability Analysis. Due to the introduction of negative stiffness springs, the proposed metamaterial beam is prone to be unstable. Therefore, it is necessary to determine the system stability. Since the infinitely long model can be regarded as the extreme case of the finitely long model, we embark on the finitely long model first.

3.3.1 Finitely Long Metamaterial Beam. By directly calculating the natural frequencies of the finitely long metamaterial beam, from the calculated natural frequencies, it can be evaluated whether the system is stable or unstable. If any of the calculated natural frequencies involves a nonzero imaginary part, the system is unstable. If all the calculated natural frequencies are pure real values, the system is stable. For the finitely long metamaterial beam, based on the assembled global governing equations (i.e., Eq. (16)), omitting the right-hand side forcing term, one can derive the natural frequencies. We consider a proposed metamaterial beam with the same parameters and properties listed in Table 1, except the beam length that is dependent on the number of cells and the

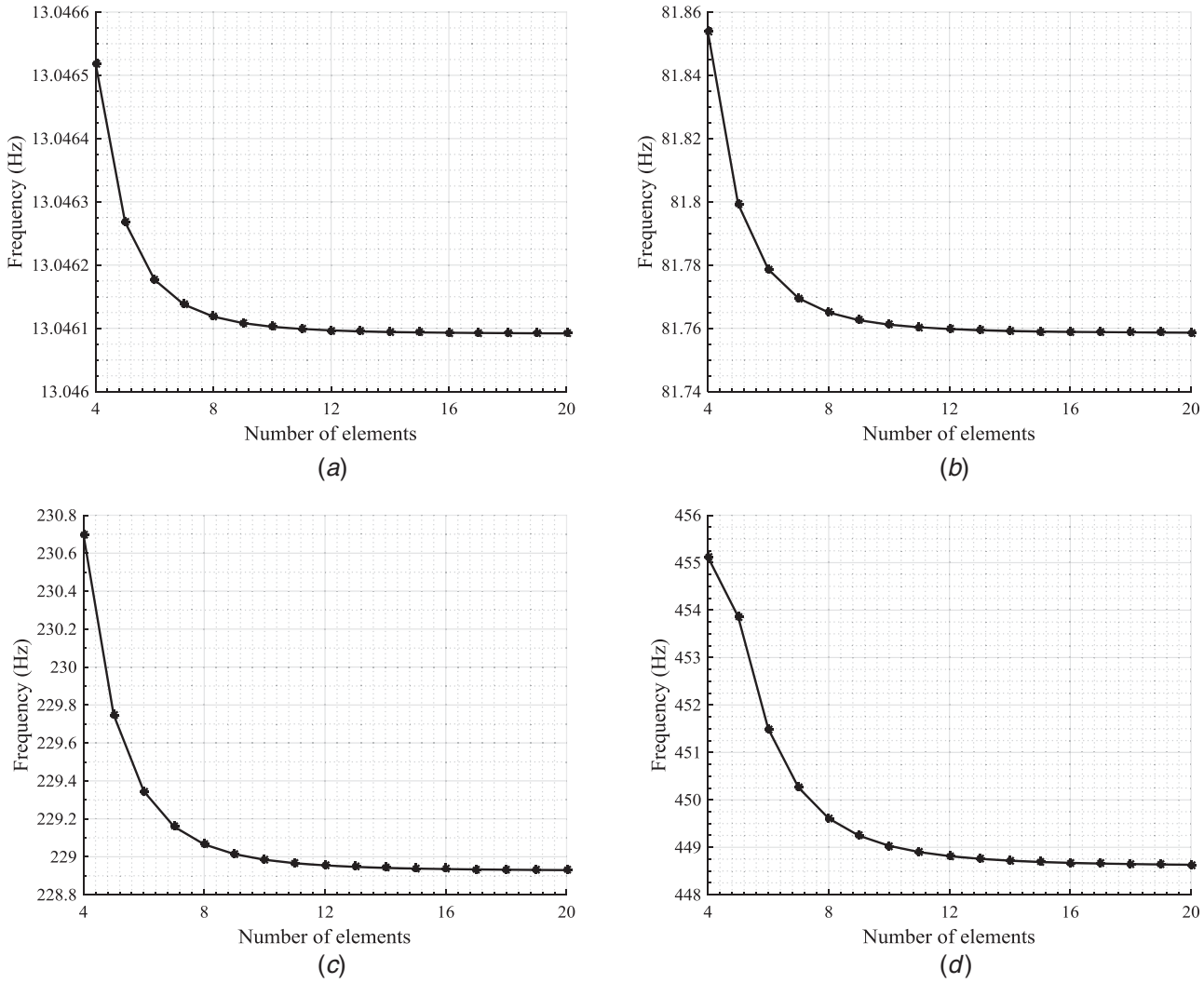

Fig. 11 Convergence plots of the first four natural frequencies with refinement of mesh: (*a*) first natural frequency, (*b*) second natural frequency, (c) third natural frequency, and (*d*) fourth natural frequency

lattice constant in the following two case studies. The parameters of the attached local resonators are $m_2 = 27.2$ g and $k_2 = 8698$ N/m. β is a dimensionless parameter with the same definition that has been introduced in the study of the lumped parameter model: $\beta = k_3/k_2$. The subscript c represents critical value.

In the first case study, the lattice constant d is 100 mm, i.e., the length of the unit cell is 100 mm or the spacing between the neighboring two local resonators is 50 mm (each unit cell contains two local resonators). Each unit cell is meshed with 10 elements, i.e., the element length is 10 mm which produces a higher mesh density than the convergence requirement. Figure 12(*a*) shows the evolution of the critical β_c with an increase in the number of cells (elements). It should be noted that for a single cell, the critical β_c is −0.483. With an increase in the number of cells, the proposed metamaterial beam is more prone to loss of stability. It can be inferred that when the number of cells is increased to infinite, i.e., the beam approaches the infinitely long metamaterial beam, the critical β_c will be 0. This means that the infinitely long metamaterial beam cannot contain any negative coupling spring. This is different from the lumped parameter model for which the stability is independent of the number of cells. This difference can be explained by the discrepancy between the lumped parameter model and the distributed parameter model which intrinsically possesses the rotation DOF in addition to the displacement DOF. For the finitely long metamaterial beam, while analyzing the stability of the single-cell system, the left-hand side of the system is assumed to be clamped. The rotation DOF of the left-hand side is completely constrained. However, when multiple cells are connected in series, the rotation DOFs of left-hand sides of the cells except the first one in the multiple-cell system are not constrained. Hence, the multiple-cell system cannot be simply regarded as an assembly of multiple identical singe-cell systems. Therefore, it can be understood why for the distributed parameter model (i.e., metamaterial beam) the stability condition of a multiple-cell system is not the same as that of a single-cell system. In addition to the number of cells, in the second case study, the effect of the lattice constant on the critical β_c is also investigated. The proposed metamaterial beam consists of 3 cells and each cell is meshed with 10 elements. Figure 12(*b*) shows the change of the critical β_c with an increase in the lattice constant. It can be observed that with an increase in the lattice constant, the proposed metamaterial beam is more prone to lose of stability.

3.3.2 Infinitely Long Metamaterial Beam. The stability of the infinitely long metamaterial beam can be determined by using the method presented in Ref. [32]. The procedure is similar to that of the lumped parameter model introduced in Sec. 2.2. By sweeping the wavenumber, one can calculate the corresponding frequencies. For any given wavenumber, if all the solutions of the corresponding frequencies are pure real values, the system is deemed to be stable. Otherwise, provided that any of the solutions of the corresponding frequencies involves a nonzero imaginary part, the system is unstable. The same mesh density is used for the infinitely long metamaterial beam to ensure the model convergence. For the corresponding infinitely long metamaterial beam with the same system parameters as those of the finitely long metamaterial beam, it is found that as long as β becomes negative, for any given wavenumber, there appears one solution of the frequency that contains a nonzero imaginary part. This is indeed expected and confirms the speculation derived from the parametric analysis of the effect of the number of cells on the critical β_c of the finitely long metamaterial beam. This indicates that to ensure stability for the infinitely long metamaterial beam, the stiffness of the coupling spring must not be tuned negative. Therefore, there is no significance to investigate the infinitely long metamaterial beam and its band gap behavior. The focus of Sec. 3.4 will be on the investigation of the finitely long model of the proposed metamaterial beam.

3.4 Transmittance Analysis. In combination with the clamped-free boundary conditions, the governing equations (i.e., Eq. (16)) of the proposed metamaterial beam consisting of limited number of cells can be solved. Detailed procedures can be referred to Ref. [32]. The transmittance is defined as the ratio of the displacement amplitude at the free end to the displacement amplitude of the base excitation. Figure 13 shows the transmittances of the proposed metamaterial beams with different β and different number of cells. It should be mentioned that the critical β_c for the metamaterial beams consisting of 3, 5, 10, and 15 cells are −0.41, −0.318, −0.157, and −0.086, respectively. From Fig. 13, it can be noted that for the cases when $\beta \neq 0$, there appears an additional vibration attenuation region in the lower frequency range. A common trend that can be observed is that with an increase in the magnitude of β, the additional vibration suppression region shifts downward to the lower frequency direction.

Figure 13(*a*) shows that for the proposed metamaterial beam consisting of three cells, when β is tuned to the critical value −0.41, a quasistatic vibration suppression region (i.e., starts from almost 0 Hz) with a considerable width is formed. This phenomenon is favorable for the realization of ultralow frequency vibration suppression. However, due to the fact that with an increase in the number of cells, the magnitude of the critical β_c decreases, i.e., the system becomes more prone to be unstable, the tunability of β

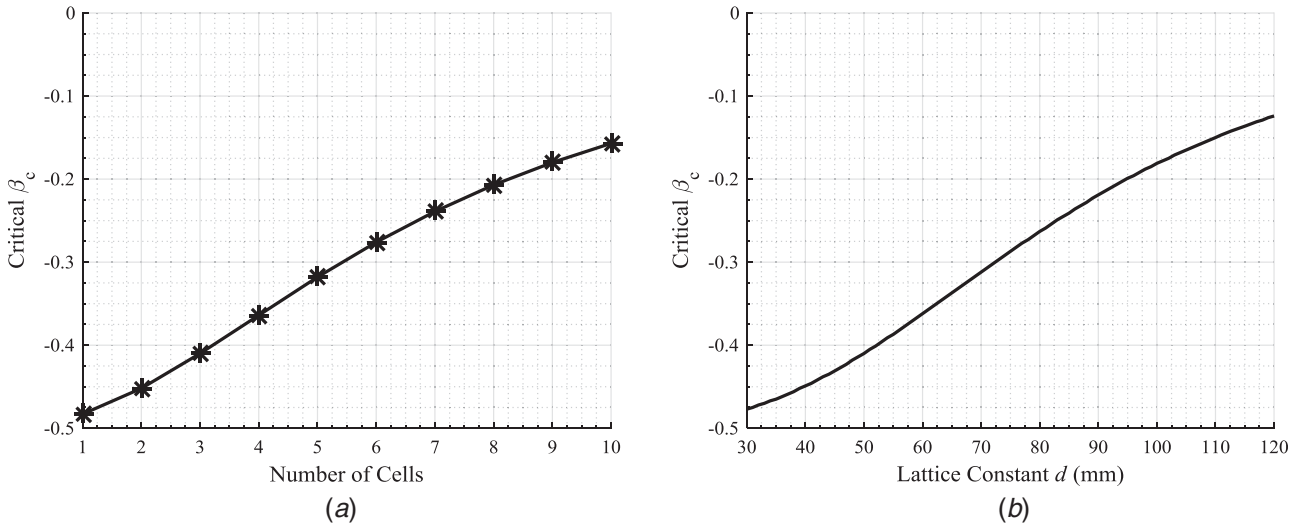

Fig. 12 Variation of β_c (*a*) with an increase in the number of cells (the lattice constant is fixed at 50 mm) and (*b*) with an increase in lattice constant (the number of cells is fixed at 6)

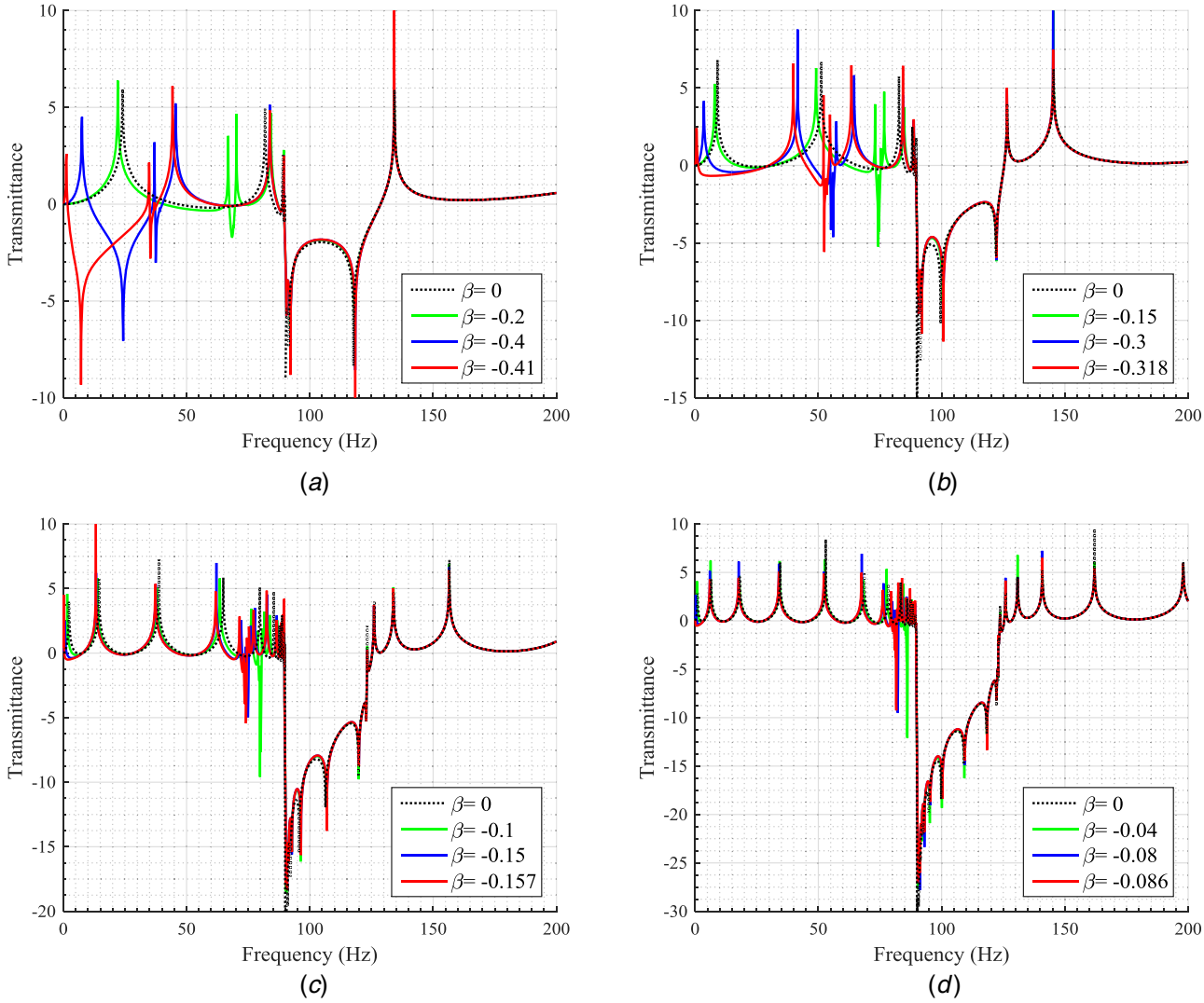

Fig. 13 Transmittances of the proposed metamaterial beam with different β and different number of cells: (*a*) 3 cells, (*b*) 5 cells, (*c*) 10 cells, and (*d*) 15 cells

is strongly restricted. Therefore, the quasistatic vibration suppression region cannot be achieved in the proposed metamaterial beam with many cells. Moreover, the additional vibration suppression region in the proposed metamaterial beam with many cells is very narrow, limiting its practical use in the circumstances where the vibation energy is spread over a wide frequency range. This poses the contradiction in the selection of the number of cells. As well known and also shown in Fig. 13, with an increase in the number of cells, the main vibration suppression region becomes deeper, indicating stronger vibration suppression ability. Recalling that the quasistatic vibration attenuation region only appears when the number of cells is small, a certain trade-off is needed for the appearance of the quasistatic vibration suppression region and the enhancement of the main vibration suppression region.

4 Further Discussion

The key of the proposed metamaterial system presented in this paper is to achieve the internal coupling by introducing negative stiffness springs. There are various ways to implement negative stiffness, depending on the characteristics of the real structures. From the literature, two main strategies for achieving negative stiffness components are buckled beams [33,34] and precompressed spring configurations [35,36]. However, the structures to achieve the above two mechanisms are relatively complicated and may not be feasible in the design of the proposed metamaterials from the mechanical perspective. Metamaterials are often required to have simple and concise forms to ensure the periodicity. Therefore, an alternative solution to realize the negative stiffness coupling for the metamaterial system is proposed based on the negative capacitance (NC) [37,38].

This mechanism using NC is inspired by the analogies between the electrical and mechanical domains. Based on the similarities between the differential governing equations in the electrical and mechanical domains, a mechanical system can be represented by an equivalent circuit and vice versa. A capacitor in the electrical domain is equivalent to a spring in the mechanical domain. By using the piezoelectric patch that couples the electrical and mechanical domains, it can be speculated that the introduction of a negative capacitance in the shunting circuit of the piezoelectric patch will be equivalent to the introduction of a negative stiffness spring in the mechanical structure. Consider a piezoelectric patch shunted to a negative capacitance C_n (Fig. 14). By using the electromechanical analogies, it can be represented by an equivalent electrical model or an equivalent mechanical model. C and K represent the capacitance and the stiffness, respectively. The subscripts n and p denote the negative capacitor and the piezoelectric patch, respectively. In fact, based on this idea, Zhu et al. [21] experimentally realized the control of Young's modulus of the piezoelectric patch through the development of a negative capacitance shunting

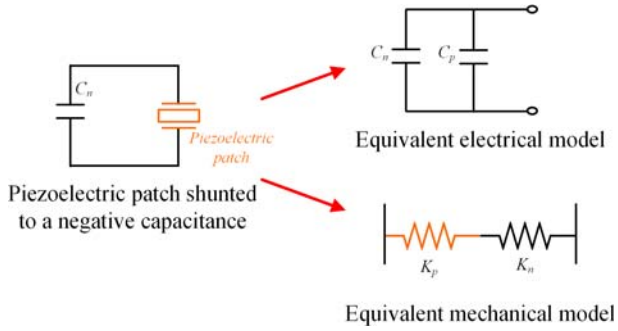

Fig. 14 Equivalent electrical and mechanical representations of a piezoelectric patch shunted to a negative capacitance

circuit. They employed the piezoelectric patches shunted to NC circuits in the design of an actively tunable metamaterial. It has been experimentally validated that the band gap of the metamaterial can be tailored by adjusting the parameters of the shunt circuits. In addition, it has been theoretically demonstrated that by carefully tuning the value of the negative capacitance, the effective stiffness introduced by the piezoelectric patch could become negative [39].

On the other hand, Li et al. [40] proposed a metamaterial system with internal coupling with adjacent piezoelectric patches coupled by LC shunt circuits. The electrical resonances in the coupled circuits aroused the band gap phenomenon in the dynamic motion of the mechanical structure. The detailed explanation on the mechanism and the mathematical derivation could be found in Ref. [40]. Inspired by the work of Zhu et al. [21] and Li et al. [40], it can be expected that a coupled circuit with negative capacitance can realize the internal coupling with negative stiffness springs between two mechanical resonators. By carefully tuning the value of the negative capacitance, the circuit-induced coupling between the two piezoelectric patches can equivalently act as a negative stiffness spring that couples the motions of the two resonators. Since the main focus of this manuscript is on the theoretical analysis of the dynamic characteristics of the proposed metamaterial, the details of the implementation will not be further discussed here.

5 Conclusions

The paper has proposed a metamaterial system with a new arrangement of local resonators. The local resonators in the proposed metamaterial system are alternately coupled by negative stiffness springs. Both the lumped parameter model (mass-in-mass structure) and the distributed parameter model (beam structure representation) of the proposed metamaterial system are studied. For the lumped parameter model, it is found that there appear three band gaps in the proposed metamaterial. A parametric study establishes that the total effective width of the band gaps is increased for the proposed metamaterial as compared to the conventional one without negative spring couplings. Moreover, by tuning the negative stiffness to the critical value, the proposed metamaterial can provide a quasistatic band gap which is favorable for realizing ultra-low frequency vibration suppression. This quasistatic band gap is also observed in the transmittance of the finite lattice model of the proposed metamaterial as a vibration suppression region.

In the distributed parameter model, the stability analysis indicates that the stiffness of the coupling spring cannot be tuned to negative values, and the quasistatic band gap cannot be achieved for an infinitely long metamaterial beam. For the practical finitely long metamaterial beam, it was found that with an increase in the number of cells and the lattice constant, the proposed metamaterial beam becomes more prone to be unstable. Within the stability regime, by designing a proposed metamaterial beam with a small number of cells, a quasistatic vibration suppression region can be potentially obtained. A trade-off is required for the selection of number of cells to ensure the appearance of the quasistatic vibration suppression region and the enhancement of the main vibration suppression region.

Acknowledgment

This work is financially supported by the Energy Education Trust of New Zealand (No. 3708242; Funder ID: 10.13039/50110000 1550) and the PhD scholarship from China Scholarship Council (No. 201608250001; Funder ID: 10.13039/501100004543).

References

[1] Brewer, G. A., 1979, "Dynamic Vibration Absorber," U.S. Patent No. 4,150,588.
[2] Alabuzhev, P., Gritchin, A., Kim, L., Migirenko, G, Chon, V., and Stepanov, P., 1989, *Vibration Protection and Measuring Systems With Quasi-Zero Stiffness*, Hemisphere Publishing, New York.
[3] McNamara, R. J., 1977, "Tuned Mass Dampers for Buildings," J. Struct. Div., **103**(9), pp. 1785–1798.
[4] Fuller, C. C., Elliott, S., and Nelson, P. A., 1996, *Active Control of Vibration*, Academic, New York.
[5] Chang, J. C., and Soong, T. T., 1980, "Structural Control Using Active Tuned Mass Dampers," J. Eng. Mech. Div., **106**(6), pp. 1091–1098.
[6] Yu, D., Wen, J., Zhao, H., Liu, Y., and Wen, X., 2008, "Vibration Reduction by Using the Idea of Phononic Crystals in a Pipe-Conveying Fluid," J. Sound Vib., **318**(1–2), pp. 193–205.
[7] Shi, Z., Cheng, Z., and Xiang, H., 2014, "Seismic Isolation Foundations With Effective Attenuation Zones," Soil Dyn. Earthquake Eng., **57**, pp. 143–151.
[8] Lu, M., Feng, L., and Chen, Y., 2009, "Phononic Crystals and Acoustic Metamaterials," Mater. Today, **12**(12), pp. 34–42.
[9] Thorp, O., Ruzzene, M., and Baz, A., 2001, "Attenuation and Localization of Wave Propagation in Rods With Periodic Shunted Piezoelectric Patches," Smart Mater. Struct., **10**(5), p. 979.
[10] Chen, S., Wang, G., Wen, J., and Wen, X., 2013, "Wave Propagation and Attenuation in Plates With Periodic Arrays of Shunted Piezo-Patches," J. Sound Vib., **332**(6), pp. 1520–1532.
[11] Hussein, M. I., Leamy, M. J., and Ruzzene, M., 2014, "Dynamics of Phononic Materials and Structures: Historical Origins, Recent Progress, and Future Outlook," ASME Appl. Mech. Rev., **66**(4), p. 040802.
[12] Liu, Z. Y., Zhang, X. X., Mao, Y. W., Zhu, Y. Y., Yang, Z. Y., Chan, C. T., and Sheng, P., 2000, "Locally Resonant Sonic Materials," Science, **289**(5485), pp. 1734–1736.
[13] Huang, H., Sun, C., and Huang, G., 2009, "On the Negative Effective Mass Density in Acoustic Metamaterials," Int. J. Eng. Sci., **47**(4), pp. 610–617.
[14] Yao, S., Zhou, X., and Hu, G., 2008, "Experimental Study on Negative Effective Mass in a 1D Mass-Spring System," New J. Phys., **10**(4), p. 043020.
[15] Liu, Y., Yu, D., Li, L., Zhao, H., Wen, J., and Wen, X., 2007, "Design Guidelines for Flexural Wave Attenuation of Slender Beams With Local Resonators," Phys. Lett. A, **362**(5), pp. 344–347.
[16] Zhu, R., Liu, X., Hu, G., Sun, C., and Huang, G., 2014, "A Chiral Elastic Metamaterial Beam for Broadband Vibration Suppression," J. Sound Vib., **333**(10), pp. 2759–2773.
[17] Nouh, M., Aldraihem, O., and Baz, A., 2014, "Metamaterial Structures With Periodic Local Resonances," Proc. SPIE, **9064**, pp. 90641Y-1–90641Y-11.
[18] Huang, G., and Sun, C., 2010, "Band Gaps in a Multiresonator Acoustic Metamaterial," ASME J. Vib. Acoust. Trans., **132**(3), p. 031003.
[19] Hu, G., Tang, L., Das, R., Gao, S., and Liu, H., 2017, "Acoustic Metamaterials With Coupled Local Resonators for Broadband Vibration Suppression," AIP Adv., **7**(2), p. 025211.
[20] Chen, S., Wang, G., and Song, Y., 2016, "Low-Frequency Vibration Isolation in Sandwich Plates by Piezoelectric Shunting Arrays," Smart Mater. Struct., **25**(12), p. 125024.
[21] Zhu, R., Chen, Y. Y., Barnhart, M. V., Hu, G. K., Sun, C. T., and Huang, G. L., 2016, "Experimental Study of an Adaptive Elastic Metamaterial Controlled by Electric Circuits," Appl. Phys. Lett., **108**(1), p. 011905.
[22] Hu, G., Tang, L., and Das, R., 2017, "Metamaterial-Inspired Piezoelectric System With Dual Functionalities: Energy Harvesting and Vibration Suppression," Proc. SPIE, **10164**, pp. 101641X-1–101641X-10.
[23] Li, X., Chen, Y., Hu, G., and Huang, G., 2018, "A Self-Adaptive Metamaterial Beam With Digitally Controlled Resonators for Subwavelength Broadband Flexural Wave Attenuation," Smart Mater. Struct., **27**(4), p. 045015.
[24] Zhou, W., Wu, Y., and Zuo, L., 2015, "Vibration and Wave Propagation Attenuation for Metamaterials by Periodic Piezoelectric Arrays With High-Order Resonant Circuit Shunts," Smart Mater. Struct., **24**(6), p. 065021.
[25] Xu, J., and Tang, J., 2017, "Tunable Prism Based on Piezoelectric Metamaterial for Acoustic Beam Steering," Appl. Phys. Lett., **110**(18), p. 181902.
[26] Yu, D., Wen, J., Shen, H., Xiao, Y., and Wen, X., 2012, "Propagation of Flexural Wave in Periodic Beam on Elastic Foundations," Phys. Lett. A, **376**(4), pp. 626–630.
[27] Lee, S. H., Park, C. M., Seo, Y. M., Wang, Z. G., and Kim, C. K., 2009, "Acoustic Metamaterial With Negative Modulus," J. Phys.: Condens. Matter, **21**(17), p. 175704.
[28] Oh, J. H., and Assouar, B., 2016, "Quasi-Static Stop Band With Flexural Metamaterial Having Zero Rotational Stiffness," Sci. Rep., **6**, pp. 33410.

[29] Drugan, W., 2017, "Wave Propagation in Elastic and Damped Structures With Stabilized Negative-Stiffness Components," J. Mech. Phys. Solids, **106**, pp. 34–45.
[30] Lyapunov, A. M., 1992, "The General Problem of the Stability of Motion," Int. J. Control, **55**(3), pp. 531–534.
[31] Hu, G., Tang, L., and Das, R., 2018, "Internally Coupled Metamaterial Beam for Simultaneous Vibration Suppression and Low Frequency Energy Harvesting," J. Appl. Phys., **123**(5), p. 055107.
[32] Hu, G., Tang, L., and Das, R., 2018, "General Framework for Modeling Multifunctional Metamaterial Beam Based on a Derived One-Dimensional Piezoelectric Composite Finite Element," J. Aerospace Eng., **31**(6), p. 04018088.
[33] Wang, Y., and Lakes, R., 2004, "Extreme Stiffness Systems Due to Negative Stiffness Elements," Am. J. Phys., **72**(1), pp. 40–50.
[34] Fulcher, B. A., Shahan, D. W., Haberman, M. R., Seepersad, C. C., and Wilson, P. S., 2014, "Analytical and Experimental Investigation of Buckled Beams as Negative Stiffness Elements for Passive Vibration and Shock Isolation Systems," ASME J. Vib. Acoust., **136**(3), p. 031009.
[35] Sarlis, A. A., Pasala, D. T. R., Constantinou, M., Reinhorn, A., Nagarajaiah, S., and Taylor, D., 2012, "Negative Stiffness Device for Seismic Protection of Structures," J. Struct. Eng., **139**(7), pp. 1124–1133.
[36] Ramlan, R., Brennan, M., Mace, B., and Kovacic, I., 2010, "Potential Benefits of a Non-Linear Stiffness in an Energy Harvesting Device," Nonlinear Dyn., **59**(4), pp. 545–558.
[37] De Marneffe, B., and Preumont, A., 2008, "Vibration Damping With Negative Capacitance Shunts: Theory and Experiment," Smart Mater. Struct., **17**(3), p. 035015.
[38] Ji, H., Qiu, J., Cheng, J., and Inman, D., 2011, "Application of a Negative Capacitance Circuit in Synchronized Switch Damping Techniques for Vibration Suppression," ASME J. Vib. Acoust., **133**(4), p. 041015.
[39] Chen, Y., Huang, G., and Sun, C., 2014, "Band Gap Control in an Active Elastic Metamaterial With Negative Capacitance Piezoelectric Shunting," ASME J. Vib. Acoust., **136**(6), p. 061008.
[40] Li, S., Xu, J., and Tang, J., 2017, "Adaptive Acoustic Metamaterial With Periodic Piezoelectric Network," Proc. SPIE, **10164**, pp. 101640N-1–101640N-10.